Analyst

Accepted Manuscript

ROYAL SOCIETY OF CHEMISTRY

www.rsc.org/analyst

Journal Name

RSCPublishing

ARTICLE

A hydrogel based nanosensor with an unprecedented broad sensitivity range for pH measurements in cellular compartments

M. Zhang,[abcd] R. V. Søndergaard,*[cd] E. K. P. Kumar,[cd] J. R. Henriksen,[de] D. Cui,[b] P. Hammershøj,[de] M. H. Clausen,[de] and T. L. Andresen[cd]

Cite this: DOI: 10.1039/x0xx00000x

Received 00th January 2012,
Accepted 00th January 2012

DOI: 10.1039/x0xx00000x

www.rsc.org/

Optical pH nanosensors have been applied for monitoring intracellular pH in real-time for about two decades. However, the pH sensitivity range of most nanosensors is too narrow, and measurements that are on the boarder of this range may not be correct. Furthermore, ratiometric measurements of acidic intracellular pH (pH < 4) in living cells are still challenging due to the lack of suitable nanosensors. In this paper we successfully developed a multiple sensor-fluorophore based nanosensor with an unprecedented broad measurement range from pH 1.4 to 7.0. In this nanosensor, three pH-sensitive fluorophores (difluoro-Oregon Green, Oregon Green 488, Fluorescein) and one pH-insensitive fluorophore (Alexa 568) were covalently incorporated into a nanoparticle hydrogel matrix. With this broad range quadruple-labelled nanosensor all physiological relevant pH levels in living cells can be measured without being too close to the limits of its pH-range. The nanosensor exhibits low susceptibility to interference by other intracellular ions at physiological concentrations. Due to its positive surface charge it is spontaneously internalized by HeLa cells and localizes to the lysosomes where the mean pH was measured at 4.6. This quadruple-labelled nanosensor perform accurate measurements of fluctuations of lysosomal pH in both directions, which was shown by treatment with the V-ATPase inhibitor bafilomycin A_1 or its substrate ATP in HeLa cells. These measurements indicate that this novel quadruple-labelled nanosensor is a promising new tool for measuring the pH of acidic compartments in living cells.

Introduction

In eukaryotic cells, compartmentalization provides distinct and functionally specialized pH environments separate from the cytosol, and pH is part of regulating the function of organelles and proteins. For example, the acidic pH of lysosomes is involved in the degradation of biomolecules like proteins and nucleic acids.[1,2] In mitochondria the difference in pH across the inner membrane is utilized to store energy.[3] Furthermore, the fluctuations of intracellular pH in living cells are recognized as a cellular regulator involved in diverse physiological and pathological processes, such as controlling the conformation and function of proteins,[4] cell proliferation and cell cycle progression.[5] It has also been shown that the low extracellular pH often observed in tumour environments is a result of increased glycolysis in the cancerous cells and that the ability to survive this low pH is linked to tumour growth.[6,7] Thus, real-time accurate quantification of the pH distribution and fluctuations in living cells will further advance our understanding of dynamic cellular processes.

Today, many pH-sensitive fluorescent indicators are identified[8] and optical monitoring of intracellular pH has conventionally been obtained by loading cells with these free dyes, thereby detecting single fluorescence intensity,[9,10] but great effort have been made to develop ratiometric fluorescent pH nanosensors.[11-14] The main advantage of measuring pH by use of ratiometric sensors is the elimination of the influence of the local concentration of the pH-sensitive fluorophores, which is otherwise impossible to control. Generally ratiometric nanosensors can be based on various matrices like silica, polymers, quantum dots and carbon nanotubes.[15,16] They covalently incorporate two or more fluorophores, usually one pH-sensitive and one pH-insensitive, to provide the ratiometric properties.[17] But also nanoparticles based on two fluorophores with opposing pH sensitivities[18] provide ratiometric properties as well as sensors based on fluorescence resonance energy transfer (FRET).[19] Generally, the nanoparticle matrices exhibit

excellent biocompatibility and shielding of the fluorophores from intracellular components like large proteins.[20] Furthermore, the covalent conjugation of the fluorophores provides full control of the fluorophore ratio and thereby the nanosensor emission ratio. Positively charged nanosensors are spontaneously internalized through endocytosis by most cells,[21] but additionally, the attachment of different ligands can drive the internalization to specific compartments in the cells. These advantages of nanoparticle based pH sensors makes them powerful tools for pH imaging in cells and other biological fluids.

Even though ratiometric measurements eliminate the influence of the local concentration of the pH-sensitive fluorophore, most ratiometric pH nanosensors are still limited by their pH sensitivity range. We previously reported a triple-labelled nanosensor incorporating two pH-sensitive fluorophores and a reference fluorophore into a nanoparticle to extend the pH sensitivity range to almost the double of conventional dual-labelled sensors containing only one pH-sensitive fluorophore.[22,23] These triple-labelled nanosensors have been used for measurements of the endosomal-lysosomal system[24] as well as for mapping the pH of the digestive system in the nematode *Caenorhabditis elegans*.[25] The sensor has a theoretical pH measurement range of 3.2 – 7.0, but the effective sensitivity range is actually only 3.6 - 6.9 as described earlier.[26] Both our measurements of lysosomal pH, when taking the full distribution of measurements into account, and the measurements by Chauhan *et al*. are approaching the lower limit of pH 3.2 and many measurements are thus in the border region between 3.2 and 3.6. As there is only an insignificant change in the optical readout at these pH values a pH distribution will look the same even though the actual pH is not. For some applications where measurements are performed on dynamic pH fluctuations or where many different treatments influencing the pH are tested, it is necessary to have a nanosensor with a sufficient pH sensitivity range. It is therefore essential to develop a new nanosensor with an even wider pH sensitivity range. A nanosensor capable of measuring pH values lower than 3 will also reveal if the lower pH values obtained in previous studies are precise or in fact even lower. Furthermore, to our knowledge, no optical pH sensor applicable for extreme acidic pH has been developed for intracellular measurements, why the pH of certain compartments is still unclear. As an example it has been reported that the pH of some large acidic vesicles in metastatic breast cancer cells is potentially lower than 4,[27] although this measurement may be questionable as it was measured with a fluorescein dye with a pK_a value of 6.5, precluding any precise measurements below pH 5.5. Furthermore, the canaliculus of gastric parietal cells functions as storage of hydrochloric acid and it was reported that the pH of this compartment is about 1.7 measured by microelectrodes.[28] There are no reports to confirm these results by optical pH nanosensors and ratiometric measurement of low pH (< 3) in living cells remains challenging.

Thus development of a nanosensor capable of covering an even wider pH range including extreme acidic pH is interesting. In this article we first present the incorporation of the pH-sensitive fluorophore difluor-Oregon Green (DFOG) in a nanosensor with two other pH-sensitive fluorophores, namely Oregon Green (OG) and Fluorescein (FA) as well as the pH-insensitive fluorophore Alexa 568. This yields a pH nanosensor with potential for measuring the full pH range of 1.4 – 7.0. Here we evaluate this quadruple-labelled nanosensor by determining its precise measurement range and its susceptibility to interference by other metal ions. After spontaneous endosomal internalization by HeLa cells we determine it to be located in lysosomes where we also perform quantification of pH by analysis of the cellular images obtained by confocal microscopy. The results indicate that the pH of lysosomes is in excellent agreement with what we have previously reported.[24] Finally, we used ATP (adenosine 5′-triphosphate disodium salt hydrate) to introduce a decrease in the normal lysosomal pH to manifest that the quadruple-labelled nanosensor is indeed capable of measuring lower pH values and is a promising tool for pH measurements of highly acidic compartments in living cells.

Results and discussion

Design and synthesis of the nanosensors

Measurements of pH with many of previously investigated optical sensors rely on the acid dissociation constant (K_a) of a pH-sensitive fluorophore. In general, the potential sensitivity range of a nanosensor is the $pK_a \pm 1$, which generates a narrow working range of maximum 2 pH units. The pH sensitivity range can be expanded by incorporating two pH-sensitive fluorophores into the nanoparticles, which have previously been reported.[22,24,29] Along with a reference fluorophore this yielded a triple-labelled nanosensor with a pH sensitivity range of almost 4 pH units. This principle of combining multiple pH-sensitive optical molecules has also been exploited by de Silva *et al*. who mixed the naked fluorescent molecules in an aqueous solution.[30]

We therefore considered that it should be possible to design and synthesize a quadruple-labelled nanosensor, with an even broader sensing pH range and the design included three pH-sensitive fluorophores with adjacent pK_a values and a reference fluorophore. For this purpose, we used the pH-sensitive fluorophores DFOG, OG and FA. In its free form DFOG has a pK_a value of 3.7,[31] however; once it is conjugated through its carboxylic acid to the amines of a nanoparticle it obtains a pK_a value of 3.0 in a dual-labelled nanosensor (one pH-sensitive and one reference fluorophore). The DFOG may thus complement the other two pH-sensitive fluorophores OG (pK_a = 4.1) and FA (pKa = 6.0) that have been used together in previous triple-labelled nanosensors and broaden the total pH-sensitive range.

The three pH-sensitive fluorophores and the reference fluorophore were covalently incorporated into a polyacrylamide cross-linked matrix as depicted in Figure 1.

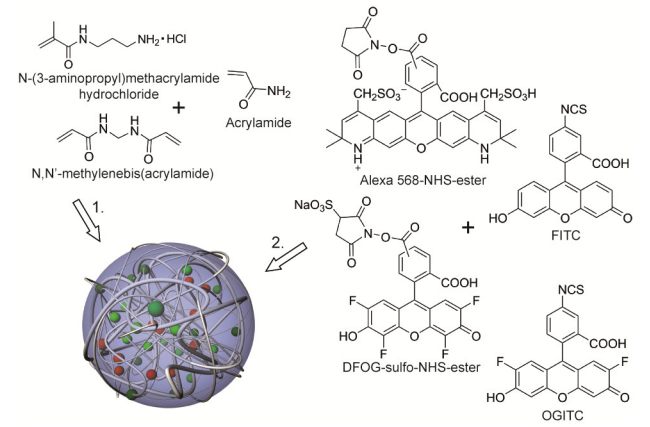

Fig. 1 Illustration of the components of the nanosensor. The nanosensor was prepared by reverse microemulsion of the different acrylamides mentioned. Hereafter, the four fluorophores were covalently attached to the free amine groups. FITC: Fluorescein isothiocyanate, DFOG: difluoro-Oregon Green, OGITC: Oregin Green isothiocyanate.

A detailed description of the synthesis of the nanoparticle and the conjugation of the fluorophores is presented in Supplementary methods. Leaching of fluorophores from the cells and from the particle is avoided by covalent binding of the fluorophores, which also ensures a constant ratio between the fluorophores in the hydrogel particle, which is important for correct ratiometric imaging. Moreover, the matrix shields the fluorophores from intracellular components like proteins, which may alter the fluorescence irrespective of pH.

pH sensitive fluorophores with other pK_a values that fits with the needs may substitute the fluorophores used in this study. The following important considerations should be taking into account; the fluorophores should have high sensitivity and specificity for protons, preferably the fluorophores should have identical excitation and emission maxima and similar quantum yields. But most importantly, the pK_a values of the pH-sensitive fluorophores should be separated by a minimum of 1.5 and a maximum of 2.0 pH units in order to obtain an extended pH range with optimal pH sensitivity throughout. A more detailed description of the design and application of multiple-labelled nanosensors have been published.[32]

Evaluation of the nanosensor

The quadruple-labelled nanosensor was mixed with buffers of ascending pH and absorbance and emission spectra were recorded. The optimal excitation wavelength for the pH sensitive fluorophores DFOG, OG and FA was determined to be 500 nm and the maximum emission intensity was collected at 523 nm. For the reference dye Alexa 568 the optimal excitation and emission wavelengths were 568 and 597 nm, respectively. Emission spectra in response to pH are presented in Supplementary Figure S1. The combined emission spectrum of the pH-sensitive fluorophores shows a pH sensitivity range from approx. 1.4 to 8.1 with a 50 fold increase in intensity. The spectrum of the reference fluorophore reveals that this fluorophore has slight pH sensitivity between 1.4 and 4.2 as well. However, the change in intensity is only 2.2 fold and as this is independent of the fluorophore concentration it will not change even though more reference fluorophores should be introduced to the nanosensor. The ratio of fluorescence emission intensities obtained at 523 and 597 nm at each pH value (F_{523}/F_{597}) canbe expressed as a function of pH. A d[ou]ble-labelled sensor with one pH-sensitive fluorophore follows a sigmoidal function described by

$$R = \frac{R_1}{10^{(pKa-pH)}+1} + R_0 \quad (1)$$

where R is the ratio of fluorescence intensities of the pH-sensitive to reference fluorophores at the corresponding pH. $R_0 = R_{min}$, the ratio for the fully protonated form and $(R_1 + R_0) = R_{max}$, the ratio for the fully deprotonated form. pK_a is the specific pK_a value of the fluorophore when incorporated into a nanoparticle matrix. Equation 1 is in accordance with what has previously been reported.[24,33] A quadruple-labelled nanosensor with three pH-sensitive fluorophores follows an extended version of equation 1:

$$R = \frac{R_1}{10^{(pKa_1-pH)}+1} + \frac{R_2}{10^{(pKa_2-pH)}+1} + \frac{R_3}{10^{(pKa_3-pH)}+1} + R \quad (2)$$

where R is the ratio (F_{523}/F_{597}) of fluorescence intensities at [a] given pH value. $R_0 = R_{min}$, the ratio for the fully deprotonated form and $(R_1 + R_2 + R_3 + R_0) = R_{max}$, the ratio for the fully protonated form. pK_a1, pK_a2 and pK_a3 are the specific pK_a values of the pH-sensitive fluorophores (DFOG, OG and FA) when conjugated into the quadruple-labelled nanosensor. The calibration curve is presented in Figure 2a where it has been normalized by subtraction of R_{min} and division by $(R_{max} - R_{min})$. We obtained the following pK_a values for the fluorophores in this quadruple-labelled nanosensor: $pK_{aDFOG} = 2.4$, $pK_{aOG} = 4.1$ and $pK_{aFA} = 6.0$. This gives us a theoretical response range of pH 1.4 - 7.0 with a 22 fold increase in ratio. As the measurements that are converted to pH are ratios between intensities any pH-sensitivity of the reference fluorophore will also be implemented in the calculation of pH. If the pH-sensitivity of the reference fluorophore is oppositely directed compared to the sensing fluorophores this will benefit the overall sensitivity range of the nanosensor. However, if the pH-sensitivity of the reference fluorophore has the same direction in the same pH interval as the sensing fluorophores, as is the case with our quadruple-labelled nanosensor, the sensitivity will be reduced. However, as the signal from the reference fluorophore only changes 2.2 fold compared to 50 fold for the sensing fluorophores this does not make a significant impact on the overall sensitivity of the nanosensor.

As mentioned, the theoretical range of this quadruple-labelled nanosensor is pH 1.4 to 7.0. However, the actual effective sensitivity range is probably smaller due to measurement uncertainties and an inherent distribution of the measurements.[26] The distribution of measurements is, among other factors, influenced by the distribution of fluorophores in the nanosensor. In our nanosensor we obtained the following R

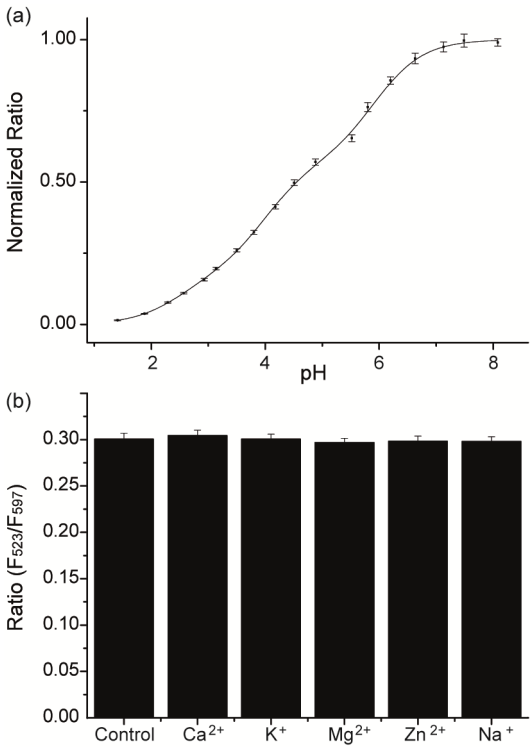

Fig. 2 (a) In vitro calibration of the quadruple-labelled nanosensor by fluorometry. Ratiometric measurements of the nanosensor in different buffers are related to pH and fitted to equation 2. The obtained ratios were normalized by subtraction of R_{min} and division by ($R_{max} - R_{min}$). Mean ± SD. (b) Influence of other ions on nanosensor signal. 1 mM of the ions was added to the buffer and the ratios of the emission intensities were measured and compared to the measurement without addition of ions (control).

values (normalized): $R_{DFOG} = 0.18$, $R_{OG} = 0.39$ and $R_{FA} = 0.43$. These numbers represent the contribution of intensity of each of the pH sensitive fluorophores that was incorporated into the particle. In the ideal sensor the R values should be as close to each other as possible.

As there is an upper limit to the total number of fluorophores that can be conjugated to a single nanoparticle, it is easy to envision that when more and more different fluorophores are introduced into the particle design, the amount of each fluorophore in each particle is decreased and the variation in number of fluorophores per particle becomes larger, relatively, than for e.g., a dual-labelled nanosensor. This complicates and reduces the repetitiveness in synthesis and therefore limits the number of different fluorophores it is reasonable to incorporate into a nanoparticle sensor. We believe that for some applications it is overall beneficial to use a quadruple-labelled nanosensor, but incorporating five or more different fluorophores will impose unmanageable complications. A more detailed description of this issue is presented in the Supplementary information along with Supplementary Figure S2, which illustrates the distribution of such measurements for this quadruple-labelled nanosensor.

Even though the biocompatible matrix of the quadruple-labelled nanosensors shields the fluorophores from interactions with intracellular macromolecules, smaller ions still interact with the fluorophores. We tested the interference of the most common intracellular ions on the response of the new nanosensor. To a buffer of pH 3.7 we added 1 mM of each of the following ions: Ca^{2+}, K^+, Mg^{2+}, Zn^{2+} and Na^+ and measured the ratio of emission intensities (F_{523}/F_{597}). The results presented in Figure 2b show that the ratio dos not change, and the calculated pH will thereby also be the same. This demonstrates that the nanosensor is not influenced by intracellular ions.

Intracellular localization of the nanosensor

The quadruple-labelled nanosensor is positively charged and is thus spontaneously internalized by HeLa cells when added to the media. We have previously shown that positively charged polyacrylamide particles are located in lysosomes after incubation for 24 hours. However, this has only been performed for a rhodamine B labelled particle and not for the full nanosensor with all pH-sensitive fluorophores.[24] The distribution of the quadruple-labelled nanosensor in HeLa cells was analyzed by colocalization with Lysotracker® Deep Red which can be separated from the fluorophores of the nanosensor (Figure 3). We observed significant co-localization as quantified by the overlap coefficient and a Pearson's correlation coefficient,[34,35] which were 0.83 and 0.85, respectively. This demonstrates that the quadruple-labelled nanosensor is located in lysosomes after 24 h.

Intracellular pH measurements

To perform intra-lysosomal pH imaging, HeLa cells were incubated with the quadruple-labelled nanosensor for 24 hours and imaged by confocal microscopy. Along with the experiment a pH calibration curve is obtained of the nanosensor in buffers with different pH values on the confocal microscope with the same settings as for the cell images. The emission intensity ratio of each pixel in an image is then converted to a pH value via the calibration curve and a histogram of pH can be constructed as well as images coloured according to a pH colour scale. Figure 4a shows measurements in HeLa cells before and after different treatments. The upper panel shows raw fluorescence images of cells with an overlay of the green and red channels and in the bottom panel are the same cells presented, coloured according to a linear pH scale. Figure 4b shows pH histograms of the measurements presented in the images of Figure 4a. Between five experiments the mean pH of the untreated cells is 4.6 ± 0.1 (mean ± SEM (Standard error of the mean), n = 5). This is consistent with what we have previously reported.[24] In this paper we utilized an identical nanoparticle matrix and obtained comparable size and zeta potential measurements. We therefore believe that our previously reported cytoxicity data and intracellular calibration are applicable to the present quadruple-labelled nanosensor. These data revealed no cytotoxicity at the employed concentration and no difference between intracellular and buffer calibration, indicating that the nanosensor is not influenced by intracellular macromolecules.[24]

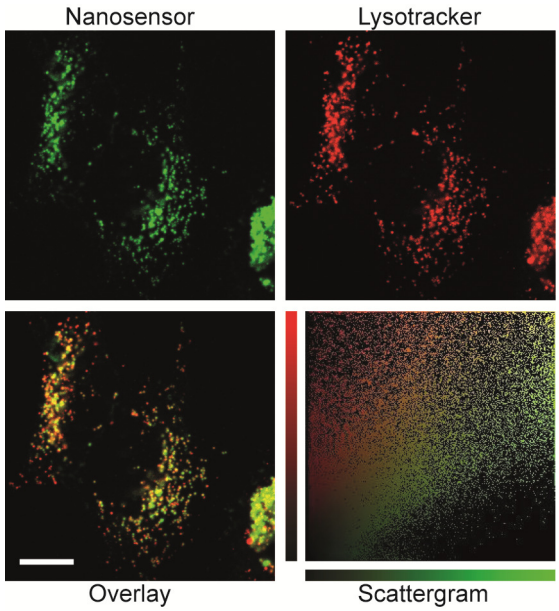

Fig. 3 Location of nanosensor in HeLa cells. Co-localization of the quadruple-labelled nanosensor (green channel) with Lysotracker® Deep Red (red channel). HeLa cells were treated with the nanosensor for 24 h and thus incubated with the Lysotracker for 30 min. before they were observed by confocal microscopy. Scale bar, 15 µm. representative of three independent experiments.

In order to illustrate that this new quadruple-labelled nanosensor is indeed able to measure changes in pH in both directions we treated the cells with either an inhibitor or an activator of the Vacuolar–type H^+-ATPase (V-ATPase),[36] which is responsible for acidification of the lysosomes. The cells were either treated with the inhibitor bafilomycin A_1 that should result in an increased pH[37] or with ATP thereby increasing the action of the V-ATPase and thus decreasing lysosomal pH.[38] From the pH images of Figure 4a it is observed that the pseudo colour of the cells treated with bafilomycin A_1 turned blue, whereas the ATP treated cells are more yellow compared to the green colour of the untreated cells. From the pH frequency histograms in Figure 4b the pH of the bafilomycin A_1 treated cells is 5.9 ± 0.0 (mean ± SEM, n = 5) and the mean pH of the ATP treated cells is 3.9 ± 0.1 (mean ± SEM, n = 4). Both of them significantly different form the mean pH of the untreated cells.

The ATP was added to the medium as the disodium salt hydrate. In order to test that the observed decrease in pH was due to the ATP and not the increased concentration of sodium or the increased osmolarity of the solution, we tested the effect of treating cells with an equivalent amount of Na_2SO_4. With a mean pH of 4.7 ± 0.1 (mean ± SEM, n = 4) this sample showed no significant difference in pH when compared to untreated cells, which indicates that neither the high sodium concentration nor the high osmolarity of the ATP sample are responsible for the observed change in pH. To further confirm that the decrease in lysosomal pH is due to consumption of the increased amount of ATP by the V-ATPase pump, cells were first treated with the inhibitor bafilomycin A_1 in order to block the action of the pump and then treated with ATP. The mean

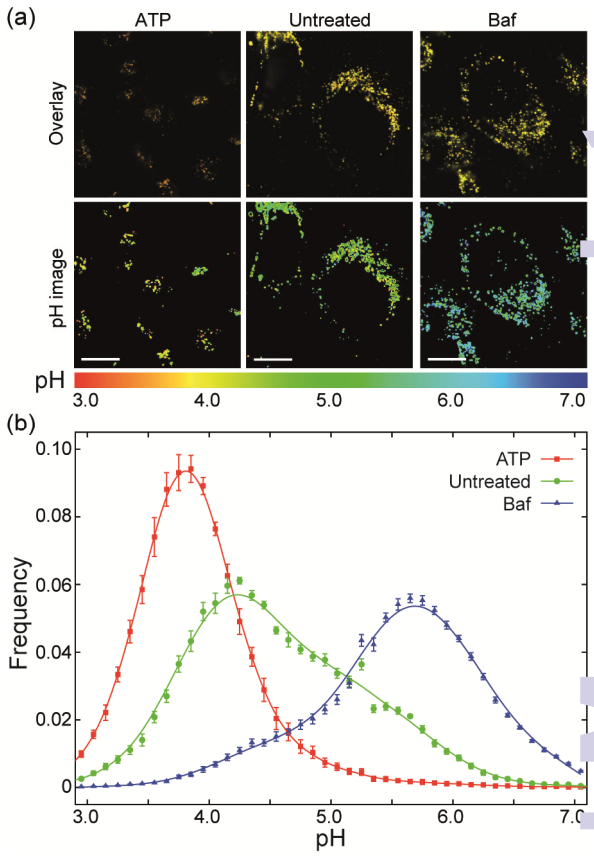

Fig. 4 pH measurements in HeLa cells. (a) HeLa cells with internalized quadruple-labelled nanosensors after 24 h were either left untreated or treated with either ATP or bafilomycin A_1 (Baf) where after they were imaged by confocal microscopy. The intensity ratios of each pixel were converted to pH via the respective calibration curve and the images were colour coded according to a common pH scale. Scale bars, 15 µm. (b) Histograms showing the pH distributions of the nanosensor signals presented in (a). Mean ± SEM (n > 5 images). No measurements are below the lower limit of the nanosensor of pH 1.4. The following percentages of measurements are above the upper limit of the nanosensor of 7.0: 0.3%, 0.8% and 15% for the ATP, untreated and Baf treated samples, respectively. Representative of four independent experiments.

pH observed for this sample was 6.0 ± 0.0 (mean ± SEM, n = 5) which is not significantly different from cells treated with bafilomycin A_1 alone. These results are presented in Figure 5 as well as in Supplementary Figure S3 and indicate that both the ATP and the bafilomycin A_1 acts directly on the V-ATPase pump, and that this pump is responsible for controlling the pH of the lysosomes.

The measurements of low pH due to treatment with ATP could have been obtained with a simpler nanosensor containing fewer pH-sensitive fluorophores. However, not knowing in advance how much the pH will drop makes it difficult to design the optimal dual- or triple-labelled nanosensor with an appropriate pH sensitivity range. Furthermore, using this quadruple labelled nanosensor enabled us to analyze the pH response to several different treatments in the same experiment with the same calibration curve. To show that the wide pH range of this quadruple-labelled nanosensor is necessary in order to perform measurements with both ATP and bafilomycin A_1 with only one sensor, we have also performed some measurements with a

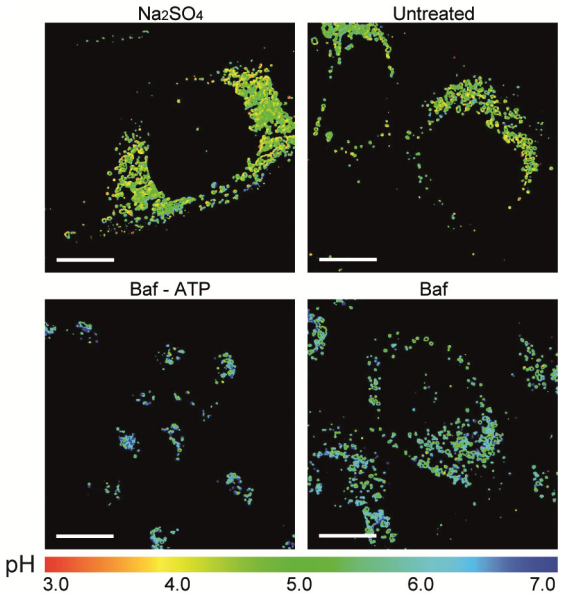

Fig. 5 Control experiments of the treatments of nanosensor containing cells. HeLa cells with internalized quadruple-labelled nanosensors for 24 h were either left untreated or treated with Na_2SO_4, bafilomycin A_1 (Baf) or bafilomycin A_1 followed by ATP (Baf – ATP). The intensity ratios of each pixel were converted to pH via the respective calibration curve and the images were colour coded according to a common pH scale. Scale bars, 15 µm. representative of four independent experiments.

triple-labelled nanosensor. These measurements are presented in Supplementary Figure S4. The nanosensor could measure the pH of untreated and bafilomycin A_1 treated cells. However, measurements performed in cells manipulated to have an intracellular pH of 3.0 could not be obtained. Since the lower limit of the triple-labelled nanosensor is 3.6, all the obtained ratios on these cells are too low to be converted to a pH. Thus the only way to present these measurements is collectively as one point at <3.6 in the pH histogram. As almost half of the pH measurements of the ATP treated cells presented in Figure 4 are below 3.6 it would not have been possible to perform these measurements with the triple-labelled nanosensor.

Conclusion

We have incorporated the pH-sensitive fluorophore DFOG into a nanoparticle matrix and determined the conjugated fluorophore to have a pK_a value of 2.4. Together with the two known pH-sensitive fluorophores OG and FA and the reference dye Alexa 568, it was incorporated into a nanoparticle to produce the novel quadruple-labelled nanosensor with a wide pH-sensitivity range from pH 1.4 to 7.0. This range covers the physiological pH range in all living cells. In HeLa cells we demonstrated that the sensor provided reliable quantitative pH measurements of the lysosomal pH with mean values ranging from pH 3.9 to 6.0 after different treatments. The acidic pH measurements in HeLa cells also highlight its potential application in real time quantification of pH in acidic compartments of many other living systems.

Experimental

Materials and reagents

BIS-TRIS propane, maleic acid, citric acid, Adenosine 5'-triphosphate disodium salt hydrate (ATP), bafilomycin A_1, Dulbecco's modified Eagle's medium (DMEM) and penicillin and streptomycin were obtained from Sigma-Aldrich. Fetal bovine serum (FBS) was obtained from Almeco A/S.

Synthesis of difluoro-Oregon Green

DFOG was prepared by acid-catalyzed condensation of 2,4-difluororesorcinol and 1,2,4-benzenetricarboxylic acid in methanesulfonic acid giving 5(6)-carboxy-2',4',5',7'-tetrafluorofluorofluorescein (DFOG) according to the procedure reported by Haugland *et al.*[31]

Characteristics of the nanoparticle employed

Synthesis of the cross-linked poly(acrylamide) nanoparticle and conjugation of fluorophores are described in the Supplemental methods. The characteristics of the employed nanosensor were analyzed by dynamic light scattering (DLS) and zeta potential measurements, carried out using a ZetaPALS analyzer (Brookhaven Instruments Corporation) yielding a size of 53 ± 3 nm and a zeta potential of 26 ± 4 mV. The obtained concentration was 6.25 mg/mL.

Characterization of nanosensor by spectrofluorometry

An in vitro calibration curve was constructed by fluorescence measurements of the nanosensor at 0.125 mg/mL in 60 mM buffers (20 mM BIS-TRIS propane (pKa: 6.8; 9.0), 20 mM citric acid (pKa 3.1; 4.8; 6.4), 20 mM maleic acid (pKa: 2.0; 6.2) and 140 mM KCl) from pH 1.4 to 8.1. Absorbance and emission spectra were obtained using an Olis upgraded SLM based spectrofluorometer to determine the optimal excitation and emission wavelengths. The calibration curve was thus obtained by excitation at 500 (pH sensitive fluorophores) and 568 nm (reference fluorophore) with emission at 523 and 577 nm, respectively. The ratio of the emission intensities at increasing pH values were plotted to produce a calibration curve.

In order to evaluate the influence of other metal ions on the nanosensor signal, 1 mM KCl, NaCl, $MgCl_2$, $CaCl_2$ or $ZnCl_2$ was added to the pH 3.7 buffer and the ratio of the emission intensities was measured and compared to the measurement without addition of ions. The osmolality of all the samples was approx. 0.3 osmol/L.

Colocalization

HeLa cells were cultured in DMEM supplemented with 10 % FBS and 100 UI/ml penicillin and streptomycin at 37 °C in a 5% CO_2 humidified incubator. For imaging, cells were kept in full growth medium without phenol red. For co-localization studies, HeLa cells were seeded in 8-well Ibidi µ-slides for 24 hours and then treated with 10 µg/mL nanosensor in full growth medium for an additional 24 hours. The cells were then washed

three times with PBS supplemented with heparin, once with PBS and kept in imaging medium for observation by confocal microscopy. For identification of lysosomes, cells were treated with 50 nM LysoTracker® Deep Red in imaging medium for 30 min. in the incubator, washed three times with PBS and kept in imaging medium for an additional 30 min. in the incubator before analysis. The nanosensor and Lysotracker were visualized by the following excitation/emission ranges 496/501-560 nm 633/700-800 nm, respectively. These excitation and emission ranges were preferred in order to exclude overlap of emissions.

Cell imaging

HeLa cells were seeded in 8-well Ibidi µ-slides for 24 hours. Once the cells were in the exponential stage, the cells were loaded with 10 µg/mL quadruple-labelled nanosensor overnight. The cells were then washed with heparin and PBS to remove surface bound nanosensors and kept in imaging medium or treated with bafilomycin A_1, ATP disodium salt hydrate or Na_2SO_4. The following treatments were performed in imaging medium: 200 nM bafilomycin A1 for 45 min. 100 mM ATP or 100 mM Na_2SO_4 for 30 min. or first 200 nM bafilomycin A_1 for 45 min. followed by 100 mM ATP. The cells were hereafter studied by confocal microscopy. The bafilomycin A_1 treated cells was the first sample to be imaged, as it was expected to yield the highest emission intensity values of the pH sensitive fluorophores due to an increase in pH. The setup of the microscope (including gain and laser power) was hereafter kept constant throughout the imaging of the following groups and calibration curve. Images were captured by a Leica TCS SP5 AOBS confocal microscope with a 63x water/immersed objective (Leica Microsystems, Germany) and sequential excitation at 496 and 561 nm with emission ranges of 501-560 nm and 566-600 nm, respectively. Two bright field images were also collected, one for each of the two laser lines, 496 and 561 nm, to correct for fluctuation in laser power.

Calibration of nanosensor by confocal microscopy

In vitro calibration curves were generated from fluorescence images of the nanosensor at 3.125 mg/mL in the same buffers as used for the characterization by spectrofluorometry. 2.5 µL of the nanosensor containing buffers at increasing pH values were transferred to a diagnostic microscopy slide and sealed with a cover glass. The microscope was focused in a plane within the solution, and images were acquired with the same settings (laser power, gain and resolution) as were employed for the imaging of cells with internalized nanosensor. Images were corrected for background by subtraction of an average value for each channel obtained by imaging of pure buffer. The fluorescence images were then corrected for laser power fluctuations by normalization with the corresponding bright field images, and mean ± SD of pixels in an image of nanosensor in buffer solution was plotted against pH values.

Image analysis

Every image series obtained in each of the cellular treatments were background subtracted according to the background obtained during calibration and images were then normalized according to the bright field images. Further image analysis was performed with a pixel by pixel analysis method as previously reported.[24] Briefly, image processing was used in order to determine which pixels are actual signal from nanosensors, and the included pixels were then converted to pH via the calibration curve. Representative images are thus re-coloured according to a linear pH colour scale and pH histograms are presented as mean ± SEM (n > 10 images).

Acknowledgements

This work was financially supported by the Lundbeck Foundation and the Novo Nordisk Foundation, Biotechnology Based Synthesis and Production Research.

Notes

[a]School of Life Sciences and Biotechnology, Shanghai Jiao Tong University, Shanghai, China.
[b]Institute of Nano Biomedicine and Engineering, Department of Instrument Science and Engineering, School of Electronic Information and Electrical Engineering, Shanghai Jiao Tong University, Shanghai, China.
[c]Department of Micro- and Nanotechnology, Technical University of Denmark, DTU Nanotech, Lyngby, Denmark.
[d]Center for Nanomedicine and Theranostics, Technical University of Denmark, Lyngby, Denmark.
[e]Department of Chemistry, DTU Chemistry, Technical University of Denmark, Lyngby, Denmark.
*E-mail: rvbe@nanotech.dtu.dk.

† Electronic Supplementary Information (ESI) available: Information on the synthesis of the nanoparticle matrix and conjugation of fluorophores to prepare the quadruple-labelled nanosensor. Furthermore, information on the width of the distributions of intensity ratios and pH histograms showing the results of the control experiments obtained by treatment of cells with either Na_2SO_4 or bafilomycin A_1 followed by ATP. See DOI: 10.1039/b000000x/

References

1 C. de Duve, *Nat. Cell Biol.,* 2005, **7**, 847-849.
2 C. Settembre, A. Fraldi, D. L. Medina and A. Ballabio, *Nat. Rev. Mol. Cell Biol.,* 2013, **14**, 283-296.
3 J. R. Casey, S. Grinstein and J. Orlowski, *Nat. Rev. Mol. Cell Biol.,* 2010, **11**, 50-61.
4 A. Schoenichen, B. A. Webb, M. P. Jacobson and D. L. Barber, *Annu. Rev. Biophys.,* 2013, **42**, 289-314.
5 L. Putney and D. Barber, *J. Biol. Chem.,* 2003, **278**, 44645-44649.
6 R. Gatenby and R. Gillies, *Nat. Rev. Cancer,* 2004, **4**, 891-899.
7 J. Chiche, K. Ilc, J. Laferriere, E. Trottier, F. Dayan, N. M. Mazure, M. C. Brahimi-Horn and J. Pouyssegur, *Cancer Res.,* 2009, **69**, 358-368.
8 J. Han and K. Burgess, *Chem. Rev.,* 2010, **110**, 2709-2728.

9 S. Ohkuma and B. Poole, *Proc. Natl. Acad. Sci. U. S. A.,* 1978, **75**, 3327-3331.
10 J. A. Thomas, R. N. Buchsbaum, A. Zimniak and E. Racker, *Biochemistry,* 1979, **18**, 2210-2218.
11 A. Ray, Y. K. Lee, T. Epstein, G. Kim and R. Kopelman, *Analyst,* 2011, **136**, 3616-3622.
12 S. M. Buck, H. Xu, M. Brasuel, M. A. Philbert and R. Kopelman, *Talanta,* 2004, **63**, 41-59.
13 T. Doussineau, S. Trupp and G. J. Mohr, *J. Colloid. Interface Sci.,* 2009, **339**, 266-270.
14 A. Schulz, J. Wotschadlo, T. Heinze and G. J. Mohr, *J. Mater. Chem.,* 2010, **20**, 1475-1482.
15 Y. E. Lee, R. Smith and R. Kopelman, *Annu. Rev. Anal. Chem.,* 2009, **2**, 57-76.
16 M. J. Ruedas-Rama, J. D. Walters, A. Orte and E. A. H. Hall, *Anal. Chim. Acta,* 2012, **751**, 1-23.
17 Desai AS, Chauhan VM, Johnston AP, Esler T and Aylott JW, *Front. Physiol,* 2014, **4**, 401.
18 P. Gong, Y. Yang, H. Yi, S. Fang, P. Zhang, Z. Sheng, G. Gao, D. Gao and L. Cai, *Nanoscale,* 2014, **6**, 5416-5424.
19 F. Du, Y. Ming, F. Zeng, C. Yu and S. Wu, *Nanotechnology,* 2013, **24**, 365101.
20 M. L. Graber, D. C. Dilillo, B. L. Friedman and E. Pastorizamunoz, *Anal. Biochem.,* 1986, **156**, 202-212.
21 T. Chung, S. Wu, M. Yao, C. Lu, Y. Lin, Y. Hung, C. Mou, Y. Chen and D. Huang, *Biomaterials,* 2007, **28**, 2959-2966.
22 H. Sun, K. Almdal and T. L. Andresen, *Chem. Commun.,* 2011, **47**, 5268-5270.
23 V. M. Chauhan, G. R. Burnett and J. W. Aylott, *Analyst,* 2011, **136**, 1799-1801.
24 R. V. Benjaminsen, H. Sun, J. R. Henriksen, N. M. Christensen, K. Almdal and T. L. Andresen, *ACS Nano,* 2011, **5**, 5864-5873.
25 V. M. Chauhan, G. Orsi, A. Brown, D. I. Pritchard and J. W. Aylott, *ACS Nano,* 2013, **7**, 5577-5587.
26 R. V. Søndergaard, N. M. Christensen, J. R. Henriksen, E. K. Pramod Kumar, K. Almdal and T .L. Andresen, *Chem. Rev.,* 2015, **115**, 8344-8378.
27 P. Montcourrier, P. H. Mangeat, C. Valembois, G. Salazar, A. Sahuquet, C. Duperray and H. Rochefort, *J. Cell. Sci.,* 1994, **107**, 2381-2391.
28 S. Schreiber, D. Garten, T. H. Nguyen, M. Konradt, R. Buecker and P. Scheid, *Cell Tissue Res.,* 2007, **329**, 313-320.
29 E. K. P. Kumar, K. Almdal and T. L. Andresen, *Chem. Commun.,* 2012, **48**, 4776-4778.
30 A. P. de Silva, S. S. K. de Silva, N. C. W. Goonesekera, H. Q. N. Gunaratne, P. L. M. Lynch, K. R. Nesbitt, S. T. Patuwathavithana and N. L. D. S. Ramyalal, *J. Am. Chem. Soc.,* 2007, **129**, 3050-3051.
31 W. C. Sun, K. R. Gee, D. H. Klaubert and R. P. Haugland, *J. Org. Chem.,* 1997, **62**, 6469-6475.
32 R. V. Søndergaard, J. R. Henriksen and T. L. Andresen, *Nat. Protoc.,* 2014, **9**, 2841-2858.
33 R. Bizzarri, C. Arcangeli, D. Arosio, F. Ricci, P. Faraci, F. Cardarelli and F. Beltram, *Biophys. J.,* 2006, **90**, 3300-3314.
34 E. M. M. Manders, F. J. Verbeek and J. A. Aten, *J. Microsc.,* 1993, **169**, 375-382.
35 A. Smallcombe, *BioTechniques,* 2001, **30**, 1240-2, 1244-6.
36 E. J. Bowman, A. Siebers and K. Altendorf, *Proc. Natl. Acad. Sci. U. S. A.,* 1988, **85**, 7972-7976.
37 T. Yoshimori, A. Yamamoto, Y. Moriyama, M. Futai and Y. Tashiro, *J. Biol. Chem.,* 1991, **266**, 17707-17712.
38 S. Ohkuma, Y. Moriyama and T. Takano, *Proc. Natl. Acad. Sci. U. S. A.,* 1982, **79**, 2758-2762.